DISCRETE AND CONTINUOUS
DYNAMICAL SYSTEMS
Volume **15**, Number **4**, August **2006**

Website: http://aimSciences.org

pp. **1035–1047**

PHASE-FIELD MODELLING OF NONEQUILIBRIUM PARTITIONING DURING RAPID SOLIDIFICATION IN A NON-DILUTE BINARY ALLOY

Denis Danilov, Britta Nestler

Karlsruhe University of Applied Sciences
Department of Computer Science
Moltkestrasse 30, D-76133 Karlsruhe, Germany

Abstract. Rapid solidification of a non-dilute binary alloy is studied using a phase-field model with a general formulation for different diffusion coefficients of the two alloy components. For high solidification velocities, we observe the effect of solute trapping in our simulations leading to the incorporation of solute into the growing solid at a composition significantly different from the predicted equilibrium value according to the phase diagram. The partition coefficient tends to unity and the concentration change across the interface progressively reduces as the solidification rate increases. For non-dilute binary alloys with a value of the partition coefficient close to unity, analytical solutions of the phase-field and of the concentration profiles are found in terms of power series expansions taking into account different diffusion coefficients of the alloy components. A new relation for the velocity dependence of the nonequilibrium partition coefficient $k(V)$ is derived and compared with predictions of continuous growth model by Aziz and Kaplan [1]. As a major result for applications, we obtain a steeper profile of the nonequilibrium partition coefficient in the rapid solidification regime for $V/V_D > 1$ than previous sharp and diffuse interface models which is in better accordance with experimental measurements (e.g. [2]).

1. **Introduction.** Recent progress in the understanding of pattern formation during solidification is associated with the development of models containing a continuous order parameter named "phase field" [3]. The phase-field models of solidification use a time and space dependent variable φ (the phase field) to describe the thermodynamic state of the various regions of the system. For example, in solid-liquid phase systems, the solid phase corresponds to $\varphi = 1$ and the liquid phase to $\varphi = 0$. Interfaces between the phases are identified by a smooth but highly localized transition of the phase-field variable in the interval $0 < \varphi < 1$. First, from a theoretical viewpoint, the phase-field approach has the advantage in providing a unified description of the system. The diffuse interface formulation allows to derive the whole set of governing equations for the bulk phases and for the interfacial regions at the same time in a thermodynamically consistent way on the basis of an entropy functional applying the first and the second law of thermodynamics [4, 5, 6]. Therefore, the evolution equations fulfill the conservation laws for mass and energy as well as a positive local entropy production. Second, the continuous phase-field variable facilitates a numerical treatment by avoiding the explicit tracking of the solid-liquid

2000 *Mathematics Subject Classification.* Primary: 41A60, 65C20; Secondary: 35K55,68U20.
Key words and phrases. Solidification, solute trapping, phase-field model, diffusion, alloys.

interface, in particular, when complex geometries are involved [3] as e.g. in the case of growing dendrites or eutectic structures.

At low growth velocities, the thickness of the diffuse interface is physically small in comparison with the characteristic length scale of the microstructure. In this case, it has been shown mathematically, that in the limit of zero interface thickness, the phase-field approach converges to classical moving boundary problems of solidification [6, 7, 8, 9]. Under rapid solidification conditions, the scale of the diffusion field becomes comparable with the interface thickness. This leads (i) to a nonequilibrium, velocity dependent partition coefficient $k_a(V) = c_S/c_L$, defined by the ratio between the concentration c_S of the growing solid and of the liquid c_L (ii) to a nonequilibrium liquidus slope and (iii) to kinetic phase diagrams within the scope of the phase-field approach [10, 11, 12].

In the dilute alloy limit, Aziz and Kaplan [1] have formulated a continuous growth model (CGM) that expresses the velocity dependence of the partition coefficient by

$$k_a(V) = \frac{k_e + V/V_D}{1 + V/V_D},$$

where k_e is the equilibrium partition coefficient. The so-called "diffusive speed" V_D is the ratio of the solute diffusivity at the interface to the interatomic distance. The CGM describes the experimentally observed solute trapping phenomenon that takes place in the rapid solidification regime when the velocity V approaches V_D. Solute atoms do not diffuse rapidly enough ahead of the growing solid phase and hence become engulfed into the advancing crystal/melt interface. Laser experiments with high processing velocities reach growth velocities of 1–10 m/s corresponding to the transition from local interfacial equilibrium to complete solute trapping, $k_a(V) \to 1$. The CGM has been applied to various dilute alloys and to process conditions in the low-velocity regime ($V \leqslant V_D$), [13, 14]. In the high-velocity regime ($V \geqslant V_D$), it can be seen in Fig. 1 that the experimental data of two Si-As alloys (open dots and solid triangles) show a much steeper profile than the CGM (solid line) proposes. Numerical results of Monte Carlo simulations [15] and of molecular dynamics simulations [16] show that a good agreement between simulated values of the non-equilibrium partition coefficient and theoretical model predictions is obtained for low and moderate interface velocities. At high growth velocities, a clear discrepancy can be observed in Fig. 2 of [15] and in Fig. 7 of [16] confirming the steeper profile suggested by the experimental data of Si-As [2]. Galenko and Sobolev [17] proposed a modification of the sharp interface model by Aziz and Kaplan [1] in order to reflect the tendency at high growth velocities.

At such length scales, diffuse interface methods are found to provide more reasonable descriptions of the diffusion processes. The phase-field method enables the modelling of the evolving bulk phases, of the phase transition from liquid to solid as well as of the velocity dependence of the jump in concentration in the interfacial region.

In this paper, we aim to derive a new definition of the non-equilibrium partition coefficient $k(V)$ on the basis of a phase-field approach. The new velocity dependence of the partition coefficient taks concentrations at the boundaries of the diffuse solid-liquid interface layer into consideration and herewith leads to a more rapid increase of the partition coefficient to one for high velocities. We assume a steeper profile for the function $k(V)$ in better accordance with experimental measurements for high growth velocities. This tendency is supported by the experimental data points of

Si-As in Fig. 1 at interface velocities $V > 1.0m/s$. Further, the new derivation of $k(V)$ is also applicable to also describe non-dilute alloy systems.

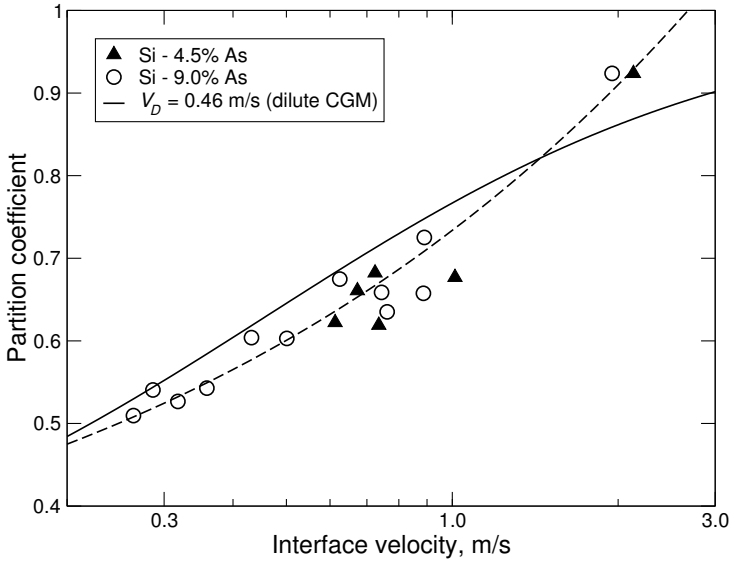

FIGURE 1. Experimentally measured partiation coefficient (open dots and solid triangles) versus interface velocity for two Si–As alloy systems in comparison with the prediction of the CGM (solid line). The data are taken from [2]. The dashed line corresponds to an interpolation curve of the experimental data.

The outline of this paper is as follows. In Sec. 2 and 3 we summerize the equations of the phase-field model that will be considered including a formulation of interdiffusion. Further, we define the leading order expansions. In Sec. 4 we apply the phase-field model to simulations of steady-state growth of a planar solid-liquid interface in non-dilute binary Ni-Cu alloys under rapid solidification conditions. A special emphasis lies on the investigation of different diffusion properties of the alloy components. The characteristical concentration profiles across the crystal/melt interface are illustrated for different growth speeds. A new relation for the velocity dependence of the partition coefficient $k(V)$ is derived and the profile is compared with previous models such as the CGM. Conclusions are drawn in Sec. 5.

2. **Phase-field model.** We use the phase-field formulation for alloy solidification that has recently been proposed in [6] for a general class of multicomponent and multiphase systems. We reduce the general case to two phases (solid and liquid) and to a binary alloy with components A and B and write down evolution equations of the phase-field model for isotropic kinetics and isotropic surface energies of the solid–liquid interface.

We assume the alloy to be at a constant temperature T in ideal solution approximation and postulate the free energy density f in the form

$$f(c,\varphi) = \sum_{i=1}^{2} c_i L_i \frac{T - T_i}{T_i} h(\varphi) + \frac{RT}{v_m} \sum_{i=1}^{2} c_i \ln c_i, \tag{2.1}$$

where L_i and T_i, $i = 1, 2$, are the latent heats and melting temperatures of the alloy components A and B, c_i are the concentrations given in molar fraction, v_m is the molar volume and R is the gas constant. The value of $\varphi = 1$ corresponds to the solid phase, $\varphi = 0$ corresponds to the liquid and the function $h(\varphi) = \varphi^2(3 - 2\varphi)$ is monotonic on the interval $[0, 1]$ satisfying the conditions $h(0) = 0$ and $h(1) = 1$.

The evolution of the phase-field variable φ is determined by the partial differential equation

$$2\omega\varepsilon\partial_t\varphi = 2\varepsilon\gamma\nabla^2\varphi - \frac{9\gamma}{\varepsilon}g_{,\varphi}(\varphi) - \frac{1}{T}f_{,\varphi}(c, \varphi), \tag{2.2}$$

where $g(\varphi) = \varphi^2(1 - \varphi)^2$ is a double well potential. By $g_{,\varphi}$ and $f_{,\varphi}$, we denote the derivative of the functions $g(\varphi)$ and $f(c, \varphi)$ with respect to φ. The model parameters ε, γ, ω are related to physical parameters of the alloy. The correlations are defined in Sec. 3.1. The diffusion mass transport of the alloy components is driven by the gradients of the chemical potential μ_i defined as

$$\mu_i = f_{,c_i} = L_i\frac{T - T_i}{T_i}h(\varphi) + \frac{RT}{v_m}(\ln c_i + 1).$$

Following nonequilibrium thermodynamics, we write the mass flux J_i as a linear function of the driving forces

$$J_i = \sum_{j=1}^{2} L_{ij}\nabla\frac{-\mu_j}{T}. \tag{2.3}$$

According to [6, 18], the phenomenological coefficients $L_{ij}(c, \varphi)$ are given by the expression

$$L_{ij}(c, \varphi) = \frac{v_m}{R}D_i c_i\left(\delta_{ij} - \frac{D_j c_j}{\sum_{k=1}^{2} D_k c_k}\right). \tag{2.4}$$

By this definition, different diffusion coefficients $D_i(\varphi)$ of the alloy components A and B are taken into account and the condition $c_1 + c_2 = 1$ is satisfied. The form of Eqs. (2.2)–(2.4) leads to a nonnegative local entropy production ensuring the second law of thermodynamics in the system.

Further, we rescale the latent heats and the melting temperatures by $\widetilde{L}$ and $\widetilde{T}$, respectively and introduce dimensionless variables λ_i, θ_i, θ via

$$\widetilde{L} = \frac{L_1 L_2}{L_1 + L_2}, \quad \widetilde{T} = \frac{T_1 T_2}{T_1 - T_2},$$
$$\lambda_i = \frac{L_i}{\widetilde{L}}, \quad \theta_i = \frac{T_i}{\widetilde{T}}, \quad \theta = \frac{T}{\widetilde{T}}.$$

The form (2.1) of the free energy density f leads to a relationship along the equilibrium phase diagram

$$-\ln\frac{c_B^S}{c_B^L} = \frac{v_m L_B}{R}\frac{T - T_B}{TT_B},$$

where c_B^S is the solidus concentration of the component B, c_B^L is the liquidus concentration, and T is the corresponding temperature on the equilibrium phase diagram. An analogous relationship holds for the component A. Thus, the dimensionless expression $v_m\tilde{L}/(R\tilde{T})$ can be considered as a scale for the "thickness" of the lense-type phase diagram, and we introduce the small parameter δ by

$$\delta = \frac{v_m\widetilde{L}}{R\widetilde{T}} \sim -\ln k_e \simeq -(k_e - 1).$$

For example, the alloy system Ni–Cu has an equilibrium partition coefficient $k_e = 0.88$ and correspondingly, $\delta = 0.14$. To find an approximate solution of the problem, we expand the concentration and the phase-field functions $c_i(x,t)$ and $\varphi(x,t)$ and the constant isothermal temperature θ in power series of the small parameter δ leading to

$$\begin{aligned} c_1(x,t) &= 1 - c^{(0)} &&- \delta c^{(1)}(x,t) &&+ O(\delta^2), \\ c_2(x,t) &= c^{(0)} &&+ \delta c^{(1)}(x,t) &&+ O(\delta^2), \\ \varphi(x,t) &= \varphi^{(0)}(x,t) &&+ \delta\varphi^{(1)}(x,t) &&+ O(\delta^2), \\ \theta &= \theta^{(0)} &&+ \delta\theta^{(1)} &&+ O(\delta^2), \end{aligned} \tag{2.5}$$

where $c^{(0)}$ is a constant initial concentration of the component B in the melt. Inserting these expansions in Eqs. (2.3) and (2.4), the mass fluxes rewrite to

$$J_2 = -J_1 = -\delta D \nabla \left(c^{(1)} + \Delta^{(c)} h(\varphi^{(0)}) \right) + O(\delta^2), \tag{2.6}$$

where the average diffusion coefficient D is a combination of the diffusion coefficients D_i for the two alloy components, given by

$$D = \frac{D_1 D_2}{(1 - c^{(0)})D_1 + c^{(0)} D_2}, \tag{2.7}$$

and the parameter $\Delta^{(c)}$ is defined by

$$\Delta^{(c)} = c^{(0)}(1 - c^{(0)}) \left(\lambda_2 \frac{\theta^{(0)} - \theta_2}{\theta^{(0)}\theta_2} - \lambda_1 \frac{\theta^{(0)} - \theta_1}{\theta^{(0)}\theta_1} \right).$$

The assumptions in Eqs. (2.1), (2.2), (2.5) and (2.6) together with the boundary conditions and the mass conservation law describe the solidification in a nondilute binary alloy in isothermal approximation.

3. **Steady-state motion of the interface.** In alloy solidification processes, there are two major growth regimes: Non-steady state growth near equilibrium and steady state growth for non-equilibrium conditions. For low undercoolings, the growth rate continuously slows as the phase transition tends to equilibrium and the concentration in the melt approaches the equilibrium liquidus composition. Growth far from the equilibrium is usually accompanied by steady state motion of the interface leading to steady state concentration profiles. In directional solidification or in laser recrystallization experiments, a constant pulling velocity or respectively a constant speed of the laser beam forces a steady state growth conditions.

We consider the liquid composition $c^{(0)}$ in Eq. (2.5) and the front velocity V as controlled parameters whereas the self-consistent temperature and the interfacial composition will be determined from the solution of Eqs. (2.1), (2.2), (2.5) and (2.6).

For a planar solid-liquid interface growing with a constant velocity V, we introduce a moving frame by

$$z = x - Vt, \tag{3.8}$$

so that the interface $\varphi = 1/2$ is located at $z = 0$. Corresponding boundary conditions which are invariant with respect to the transformation of variables are given by

$$\begin{gathered} \varphi|_{z\to-\infty} = 1, \quad \varphi|_{z\to+\infty} = 0, \\ c_1|_{z\to+\infty} = 1 - c^{(0)}, \quad c_2|_{z\to+\infty} = c^{(0)}, \quad J_i|_{z\to\pm\infty} = 0. \end{gathered} \tag{3.9}$$

In the moving frame as in Eq. (3.8), the steady-state phase field φ and the steady-state concentration fields c_i are stationary and depend only on the spatial variable z.

3.1. **Phase field.** In the zeroth order of approximation, the evolution equation for the phase field in Eq. (2.2) in the moving frame, Eq. (3.8), reads

$$2\varepsilon\gamma\varphi^{(0)}_{zz} + 2\omega\varepsilon V\varphi^{(0)}_{z} - \frac{9\gamma}{\varepsilon}g_{,\varphi}(\varphi^{(0)}) \\ - \frac{\widetilde{L}}{\widetilde{T}}\left((1-c^{(0)})\lambda_1\frac{\theta^{(0)}-\theta_1}{\theta^{(0)}\theta_1} + c^{(0)}\lambda_2\frac{\theta^{(0)}-\theta_2}{\theta^{(0)}\theta_2}\right)h_{,\varphi}(\varphi^{(0)}) = 0.$$

This equation is a nonlinear ordinary differential equation of reaction-diffusion type and together with the boundary conditions in Eq. (3.9) it has the traveling wave solution

$$\varphi^{(0)}(z) = \frac{1}{2}\left[1 - \tanh\left(\frac{3z}{2\varepsilon}\right)\right]. \tag{3.10}$$

The self-consistent temperature $\theta^{(0)}$ is defined by the relation

$$\theta^{(0)} = \frac{\theta_L}{1 + \dfrac{1}{\theta_L}\dfrac{\beta V}{\widetilde{T}}}, \tag{3.11}$$

where the temperature θ_L and the kinecelestinitic coefficient β are given by

$$\begin{aligned} \theta_L &= \frac{(1-c^{(0)})\lambda_1 + c^{(0)}\lambda_2}{(1-c^{(0)})\lambda_1/\theta_1 + c^{(0)}\lambda_2/\theta_2}, \\ \beta &= \frac{\theta_L^2}{(1-c^{(0)})\lambda_1 + c^{(0)}\lambda_2}\frac{\widetilde{T}^2}{\widetilde{L}}\omega. \end{aligned} \tag{3.12}$$

At small growth velocities V, Eq. (3.11) can be approximated by

$$\theta^{(0)} \simeq \theta_L(c^{(0)}) - \frac{\beta V}{\widetilde{T}},$$

where the last term is known as the kinetic undercooling. Using the dimensional latent heats and melting temperatures, we obtain the relations between the phase-field parameter ω and the kinetic coefficient β from Eq. (3.12) in the limit of a dilute alloy

$$\omega = \begin{cases} \beta_1 L_1/T_1^2, & c^{(0)} \to 0, \\ \beta_2 L_2/T_2^2, & c^{(0)} \to 1, \end{cases} \tag{3.13}$$

where β_0 and β_1 are the kinetic coefficients of the pure A and B substance, respectively. The entropy contribution of the solid-liquid interface is given by the integral

$$-\int_{-\infty}^{\infty}\left(\varepsilon a(\nabla\varphi^{(0)}) + \frac{1}{\varepsilon}W(\varphi^{(0)})\right)dz = -\gamma,$$

where $a(\nabla\varphi) = \gamma(\nabla\varphi)^2$ is the gradient term and $W(\varphi) = 9\gamma g(\varphi)$ is the double well potential.

Thus, the parameter γ is the surface entropy density of the solid-liquid interface related to the surface energy density σ by

$$\gamma = \frac{\sigma}{T}.$$

The parameter ω is related to the kinetic coefficient β by Eqs. (3.12) and (3.13) and the thickness of the diffuse interface is equal to 2ε because the phase-field variable $\varphi^{(0)}$ varies from 0.05 to 0.95 in the interval $-\varepsilon < z < +\varepsilon$.

3.2. **Concentration field.** For the case of steady-state interface motion, the conservation laws for the alloy components $\partial_t c_i + \nabla J_i = 0$ in the moving frame, Eq. (3.8), read

$$-V(c_i)_z + (J_i)_z = 0.$$

Taking into account the boundary conditions in Eq. (3.9) and the series expansions in Eq. (2.5), this equation integrates as follows

$$-V\delta c^{(1)} - J_1 = -V\delta c^{(1)} + J_2 = 0. \tag{3.14}$$

Since the mass fluxes disappear far from the interface, $J|_{z\to\pm\infty} = 0$, equation (3.14) leads to the relations $c^{(1)} = 0$ at $z \to \pm\infty$ and $c_i|_{z\to-\infty} = c_i|_{z\to+\infty}$.

Substituting the expression for the mass fluxes in Eq. (2.6) into the conservation law (3.14), we get the differential equation for the function $c^{(1)}$ describing the concentration profile

$$Dc_z^{(1)} + Vc^{(1)} + D\Delta^{(c)}h_{,\varphi}(\varphi^{(0)})\varphi_z^{(0)} = 0.$$

The corresponding solution satisfying the boundary conditions in Eq. (3.9) has the form

$$c^{(1)}(z) = -\Delta^{(c)}\int_{-\infty}^{z}\exp\left(-\int_y^z\frac{Vdx}{D(x)}\right)h_{,\varphi}(\varphi^{(0)})\varphi_y^{(0)}dy, \tag{3.15}$$

where $D(x) = D(\varphi^{(0)}(x))$.

4. Application to rapid solidification of non-dilute Ni-Cu alloys.

4.1. **Intrinsic length scales.** Three different length scales are present in the solution of the phase-field in Eq. (3.10) and of the concentration field in Eq. (3.15). The first length scale, ε is associated with the thickness of the diffuse solid-liquid interface. The next two scales are diffusion lengths $l_i = D_i/V$, $i = 1, 2$ determined by the diffusion properties D_i of the alloy components and by the growth velocity V. To show how these scales influence the redistribution of the alloy components, we assume for simplicity that the diffusion coefficients D_i do not depend on a spatial coordinate. Introducing a dimensionless coordinate $\xi = z/\varepsilon$, the solution in Eq. (3.10) for the phase field reads

$$\varphi^{(0)}(\xi) = \frac{1-\tanh(3\xi/2)}{2},$$

and the concentration profile in Eq. (3.15) can be rewritten as

$$\begin{aligned} c^{(1)}(\xi) &= -\Delta^{(c)}\exp\left(-\frac{\varepsilon}{l_D}\xi\right)\int_{-\infty}^{\xi}\exp\left(\frac{\varepsilon}{l_D}\eta\right)h_{,\varphi}(\varphi^{(0)})\varphi_\eta^{(0)}d\eta \\ &= -\Delta^{(c)}\exp\left(-\frac{V}{V_D}\xi\right)\int_{-\infty}^{\xi}\exp\left(\frac{V}{V_D}\eta\right)h_{,\varphi}(\varphi^{(0)})\varphi_\eta^{(0)}d\eta, \end{aligned} \tag{4.16}$$

where we set

$$\begin{aligned} l_D &= \frac{D}{V} = \frac{l_1 l_2}{(1-c^{(0)})l_1 + c^{(0)}l_2}, \\ V_D &= \frac{D}{\varepsilon} = \frac{V_1 V_2}{(1-c^{(0)})V_1 + c^{(0)}V_2}. \end{aligned} \tag{4.17}$$

As can be seen from Eq. (4.16), the concentration field $c^{(1)}$ depends on the relation between the interface length ε and the diffusion length l_D or, reformulated, on the relation of growth velocity V and diffusion speed V_D. The parameters l_D and V_D are functions of the melt composition $c^{(0)}$ and include the corresponding quantities $l_i = D_i/V$ and $V_i = D_i/\varepsilon$ of the alloy components A and B.

For the subsequent computations, we adopt a set of physical parameters corresponding to the Ni–Cu binary alloy. The following thermophysical properties have been assumed: $T_{\mathrm{Ni}} = 1728\,\mathrm{K}$, $T_{\mathrm{Cu}} = 1358\,\mathrm{K}$, $L_{\mathrm{Ni}} = 2350\,\mathrm{J/cm^3}$, $L_{\mathrm{Cu}} = 1728\,\mathrm{J/cm^3}$, $v_m = 7.42\ \mathrm{cm^3}$. For the dynamical properties (diffusion and kinetic coefficients), the results of molecular dynamics simulations reported in [19] have been used: $D_{\mathrm{Ni}} = 3.82 \times 10^{-9}\ \mathrm{m^2/s}$, $D_{\mathrm{Cu}} = 3.32 \times 10^{-9}\ \mathrm{m^2/s}$, $\beta = 2.22\,\mathrm{K\,s/m}$. The parameter ε is set to $\varepsilon = 0.4$ nm leading to a diffuse interface of thickness $2\varepsilon = 0.8$ nm.

As noted above, we consider the melt composition $c^{(0)}$ and the velocity of the planar front V as two control parameters. Fig. 2 shows the phase-field profile $\varphi^{(0)}$ (dashed line) and the three concentration profiles $c^{(1)}(\xi)$ for different growth velocities and for a fixed melt composition $c^{(0)} = 0.5$. The vertical dotted lines at $\xi = \pm 1$ correspond to the boundaries of the diffuse interface region $0.05 \leq \varphi^{(0)} \leq 0.95$ between the solid and liquid phases. $\xi = 0$ is the position of the interface at $\varphi^{(0)} = 0.5$.

Three changes in the concentration profile can be seen with increasing growth velocity: (i) the concentration gradient in the liquid phase increases; (ii) the difference between the concentrations of the solid and liquid decreases; (iii) the maximum $c^{(1)}_{\max}$ of the concentration profile shifts its position $\xi_{\max}$ from about $\xi_{\max} = 1$ to $\xi_{\max} = 0$, see also Fig. 3. These changes render a depression of the concentration boundary layer in front of the growing interface with increasing front velocity. At low growth velocities with $V/V_D = 0.1$, the diffusion length l_D is larger than the interface scale ε and a pronounced concentration boundary layer is present in the liquid phase in Fig. 2a. At high growth velocities with $V/V_D = 10$, the diffusion length l_D is smaller than the interface scale ε. Hence, the inhomogeneity of the concentration field $c^{(1)}$ is completely contained in the diffuse interface region at $-1 \leqslant \xi \leqslant 1$. The liquid phase at $\xi > 1$ has the uniform composition $c^{(0)}$ (Fig. 2c).

To emphasize the effect of different diffusion coefficients D_i and of the composition dependence $D(c^{(0)})$ on the concentration field $c^{(1)}$, we consider strongly different values for the diffusion properties of alloy components, namely $D_1 = 3 \times 10^{-9}\ \mathrm{m^2/s}$ and $D_2 = 0.1 D_1 = 3 \times 10^{-10}\ \mathrm{m^2/s}$.

The nonlinear function $\zeta(c) = D(c)/D_1 = l_D(c)/l_1 = V_D(c)/V_1$ represents the dependence of the diffusion coefficient $D(c)$ in Eq. (2.7) or equivalently of the diffusion length $l_D(c)$ or of the diffusion speed $V_D(c)$ in Eq. (4.17) on the melt composition c. The behaviour of $\zeta(c)$ versus the concentration c is shown in Fig. 4.

In Fig. 5, we present concentration profiles $c^{(1)}$ (scaled by $c^{(1)}_{\max}$ for convenience) at a fixed growth velocity for three different melt compositions $c^{(0)}$. In the case of a melt composition with small amount of component B, e.g. $c^{(0)} = 0.1$, the decay of the concentration boundary layer is determined by the diffusion coefficient $D_B = D_2$ and correspondingly by the length scale l_2 (Fig. 5a). In the opposite case of a B-atom rich melt, e.g. $c^{(0)} = 0.9$, the diffusion process is determined by the diffusion coefficient $D_A = D_1$ and by the length scale l_1 (Fig. 5c). The intermediate case of nondilute alloy composition $c^{(0)} = 0.5$ is described by the weighted diffusion

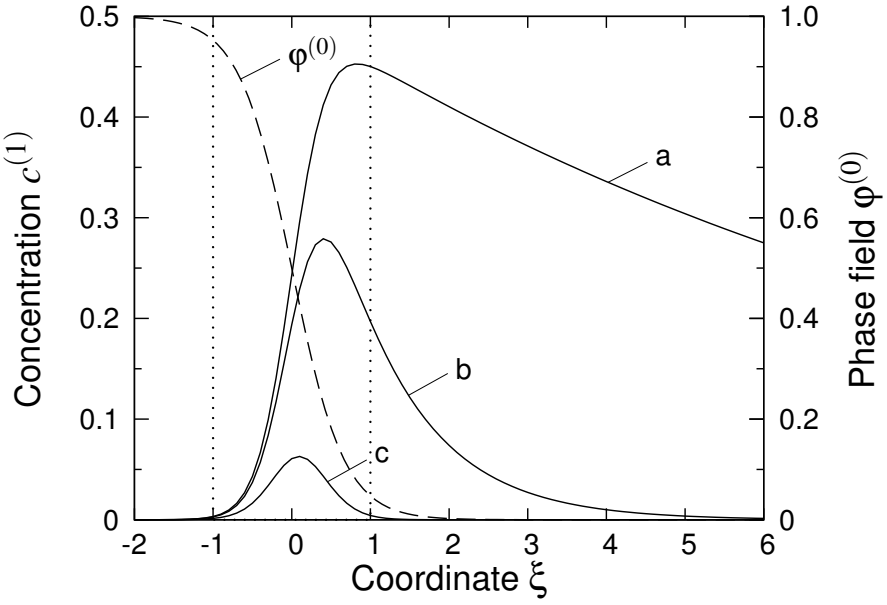

FIGURE 2. Steady-state profiles $c^{(1)}$ of Eq. (4.16) for $c^{(0)} = 0.5$ and for three different growth velocities: (a) $V = 0.89$ m/s and $\varepsilon/l_D = V/V_D = 0.1$; (b) $V = 8.9$ m/s and $\varepsilon/l_D = V/V_D = 1$; (c) $V = 89$ m/s and $\varepsilon/l_D = V/V_D = 10$.

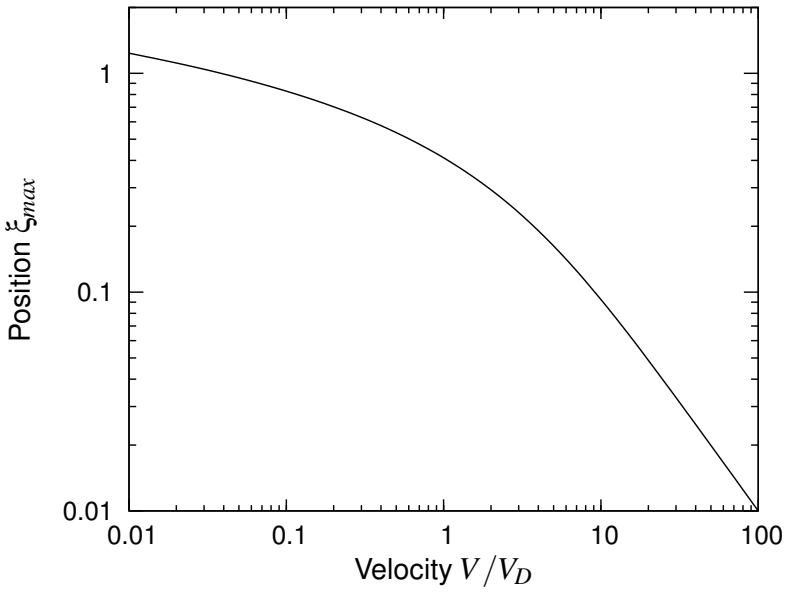

FIGURE 3. Dependence of the position $\xi_{\max}$ of the maximum $c^{(1)}_{\max}$ in the concentration profile on the growth velocity V.

coefficient D which depends on both, D_1 and D_2, according to Eq. (2.7), Fig. 5b.

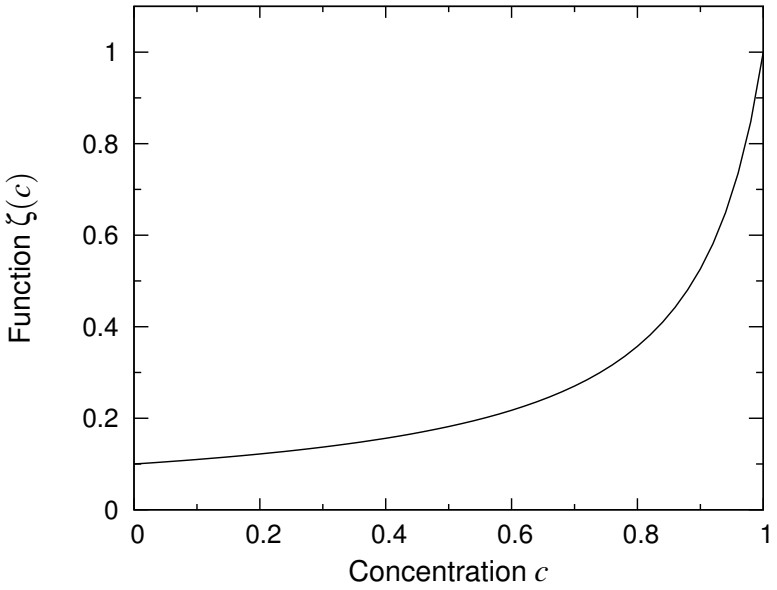

FIGURE 4. Nonlinear dependence of the quantities D, l_D and V_D on the melt composition.

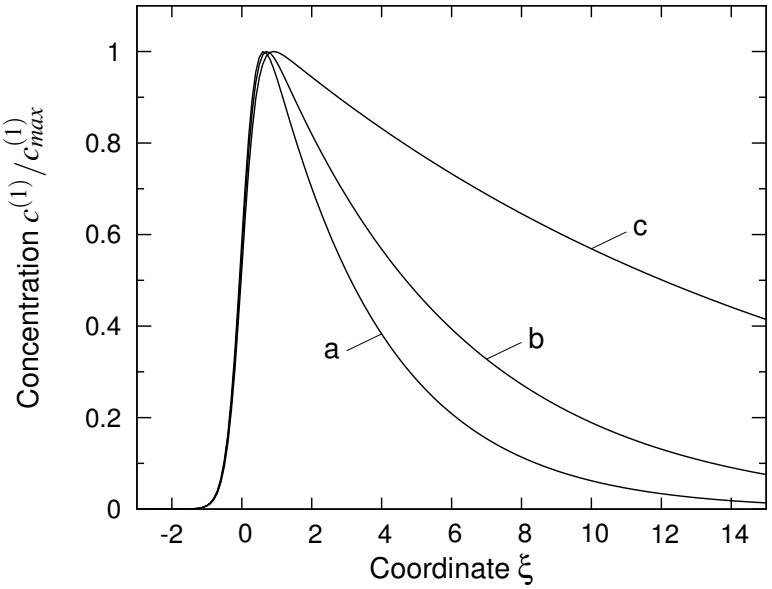

FIGURE 5. Steady-state concentration profile $c^{(1)}/c^{(1)}_{\max}$ at a fixed growth velocity $V = 0.25$ m/s for different melt compositions $c^{(0)}$: (a) $c^{(0)} = 0.1$, (b) $c^{(0)} = 0.5$, (c) $c^{(0)} = 0.9$.

4.2. **Nonequilibrium partition coefficient.** The partition coefficient k of an alloy component is defined by the ratio between its concentration in the growing solid phase c_S and that in the liquid phase c_L at the interface. Experiments show

that, with increasing interface velocity, the partition coefficient increases from its equilibrium value k_e [13] and approaches unity under rapid solidification conditions [2]. This phenomenon has been termed "solute trapping".

In this section, the partition coefficient of the component B that follows from the solution in Eq. (3.15) is compared with the prediction of the continuous growth model in [1], where the dependence of the partition coefficient k_a on the interface velocity V has been derived as

$$k_a(V) = \frac{c_2^S}{c_2^L} = \frac{k_e + V/V_D}{1 + V/V_D}. \tag{4.18}$$

Considering Fig. 2, two definitions of the partition coefficient in the phase-field formulation are possible. In the first case, the concentration of B-atoms in the liquid at the interface is associated with the maximum of $c^{(1)}$ and the concentration in solid is assumed equal to $c^{(0)}$. Taking into account the expansion in Eq. (2.5), this leads to a partition coefficient k_m that reads

$$k_m = \frac{c_2|_{\xi\to\infty}}{c_2|_{\xi=\xi_{\max}}} = \frac{c^{(0)}}{c^{(0)} + \delta c^{(1)}_{\max}}. \tag{4.19}$$

This definition of the partition coefficient has been used in the articles [10, 11] where it is applied to dilute binary alloys. In the second case, we define the concentrations in the solid and liquid phases at the corresponding boundaries of the diffuse interface, i.e. at $\xi = \pm 1$, by $c_2^S = c_2|_{\xi=-1}$ and $c_2^L = c_2|_{\xi=+1}$ respectively, which leads to a partition coefficient

$$k = \frac{c_2|_{\xi=-1}}{c_2|_{\xi=+1}} = \frac{c^{(0)} + \delta c^{(1)}|_{\xi=-1}}{c^{(0)} + \delta c^{(1)}|_{\xi=+1}}. \tag{4.20}$$

The three functions given by Eqs. (4.18)–(4.20) are shown in Fig. 6. For growth velocities up to $0.5V_D$, the values of the functions k_a and k coincide, while the function k_m predicts slightly smaller values of the partition coefficient. Further, at $V > 0.5V_D$, the function k tends to unity more rapidly than the functions k_a and k_m. If we compare the differently defined partition coefficients at a velocity $V = 10V_D$, we obtain the values $1 - k = 1 \times 10^{-3}$, $1 - k_a = 1.1 \times 10^{-2}$ and $1 - k_m = 1.7 \times 10^{-2}$. A value of $1 - k_a = 1 \times 10^{-3}$ for the continuous growth model is reached only at significantly large velocity $V = 120V_D$. As illustrated in the previous section in Fig. 2, the inhomogeneity of concentration field has the length comparable to, or smaller than the thickness of the diffuse interface in the case of rapid solidification conditions, i.e. at growth velocities $V \gg V_D$. Consequently, the concentration of the alloy components in the solid and in the liquid phase outside the interfacial region is uniform and equal to the initial concentration in the melt, i.e. the complete solute trapping occurs.

5. **Conclusion.** A phase-field model for non-dilute binary alloys with a general formulation of interdiffusion processes for the two components has been examined in the rapid solidification regime. Steady-state solutions for the phase field and for the concentrations of the alloy components, Eqs. (3.10) and (3.15), are obtained in terms of power series expansions under the assumption that the partition coefficient is close to unity. Simulated concentration profiles corresponding to the Ni–Cu data set show that the displacement of the concentration peak ahead of the solid-liquid interface decreases for increasing solidification rates. Further, the effect

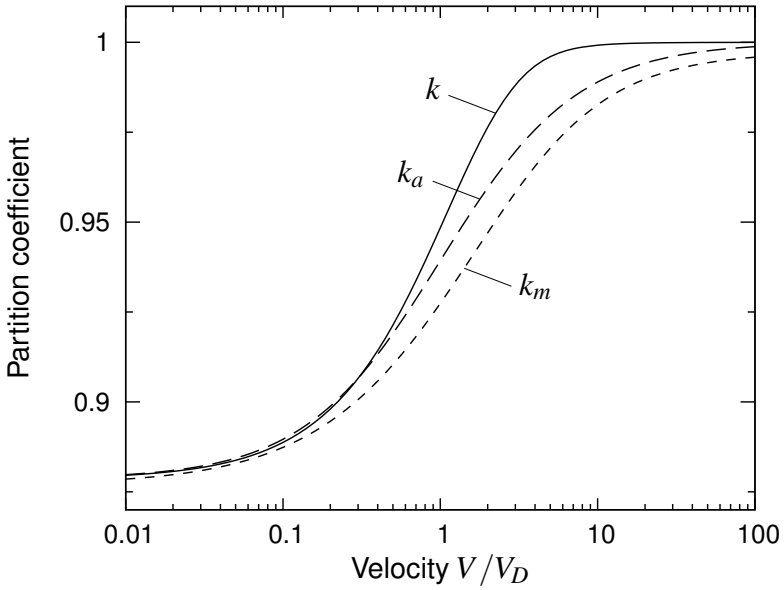

FIGURE 6. Nonequilibrium partition coefficient of the component B for the melt composition $c^{(0)} = 0.5$ as a function of the growth velocity V.

of different diffusion coefficients of the two components on the concentration profile at three positions of the binary phase diagram representing a transition from dilute to non-dilute composition are discussed. A new expression for the velocity dependence of the nonequilibrium partition coefficient, introduced by Eq. (4.20), has been derived leading to a more pronounced solute trapping effect for velocities $V/V_D > 1$. The proposed profile of the k versus V/V_D curve in Fig. 6 performs a steeper profile of partition coefficients at high soldification rates for non-dilute alloys (e.g. see [2]) than previous models. This is in accordance with the experimental data points of Si-As in [2], the numerical and theoretical predictions in [15, 16, 17]. A comparison with both, the prediction of the continuous growth model [1] given by Eq. (4.18), and the value obtained from the definition of Eq. (4.19) which is based on the concentration maximum $c^{(1)}_{\max}$ is shown. The presented model for nonequilibrium interface kinetics during rapid solidification will be applied to recover the experimental results of non-dilute Si-As alloys described in [2] in a forthcoming paper.

6. **Acknowledgments.** This work was supported by the German Research Foundation (DFG) under the priority research program 1120: "Phase transformations in multi-component melts", Grant No. Ne 822/2. The funding is gratefully acknowledged.

REFERENCES

[1] M. J. Aziz, T. Kaplan, *Continuous growth model for interface motion during alloy solidification*, Acta Metall. **36 (8)** (1988), 2335–2347.

[2] J. A. Kittl, M. J. Aziz, D. P. Brunco, M. O. Thompson, *Nonequilibrium partition during rapid solidification of Si–As alloys*, J. Cryst. Growth **148** (1995), 172–182.

[3] W. J. Boettinger, J. A. Warren, C. Beckermann, A. Karma, *Phase-field simulation of solidification*, Annu. Rev. Mater. Res. **32** (2002), 163–194.
[4] Z. Bi, R. F. Sekerka, *Phase-field model of solidification of a binary alloy*, Physica A **261** (1998), 95–106.
[5] C. Charach, P. C. Fife, *On thermodynamically consistent schemes for phase field equations*, Open Systems and Information Dynamics **5 (2)** (1998), 99–123.
[6] H. Garcke, B. Nestler, B. Stinner, *A diffuse interface model for alloys with multiple components and phases*, SIAM J. Appl. Math. **64 (3)** (2004), 775–799.
[7] G. Caginalp, W. Xie, *Phase-field and sharp-interface alloy models*, Phys. Rev. E **48 (3)** (1993), 1897–1909.
[8] K. R. Elder, M. Grant, N. Provatas, J. M. Kosterlitz, *Sharp interface limits of phase-field models*, Phys. Rev. E **64** (2001), 021604.
[9] D. Kessler, *Sharp interface limits of a thermodynamically consistent solutal phase field model*, J. Cryst. Growth **224** (2001), 175–186.
[10] A. A. Wheeler, W. J. Boettinger, G. B. McFadden, *Phase-field model of solute trapping during solidification*, Phys. Rev. E **47 (3)** (1993), 1893–1909.
[11] N. A. Ahmad, A. A. Wheeler, W. J. Boettinger, G. B. McFadden, *Solute trapping and solute drag in a phase-field model of rapid solidification*, Phys. Rev. E **58 (3)** (1998), 3436–3450.
[12] K. Glasner, *Solute trapping and non-equilibrium phase diagram for solidification of binary alloys*, Physica D **151** (2001), 253–270.
[13] M. J. Aziz, J. Y. Tsao, M. O. Thompson, P. S. Peercy, C. W. White, *Solute Trapping: Comparison of Theory with Experiment*, Phys. Rev. Lett. **56 (23)** (1986), 2489–2492.
[14] D. E. Hoglund, M. J. Aziz, S. R. Stiffler, M. O. Thompson, J. Y. Tsao, P. S. Peercy, J. Crystal Growth **109** (1991), 107.
[15] Kirk M. Beatty, Kenneth A. Jakson, *Monte Carlo modeling of dropant sergregation*, J. Cryst. Growth **271** (2004) 495-512.
[16] Franck Celestini, Jean-Marc Debierre, *Nonequilibrium molecular dynamics simulation of rapid directional solidification*, Phys. Rev. B **62(21)** (2000), 14006-14011.
[17] Peter Galenko, Sergei Sobolev, *Local nonequilibrium effect on undercooling on rapid solidification of alloys*, Phys. Rev E **55(1)** (1997), 343-352.
[18] C. M. Elliott, H. Garcke, *Diffusional phase transitions in multicomponent systems with a concentration dependent mobility matrix*, Physica D **109 (3-4)** (1997), 242–256.
[19] J. J. Hoyt, B. Sadigh, M. Asta, S. M. Foiles, *Kinetic phase-field parameters for the Cu-Ni system derived from atomistic computations*, Acta mater. **47 (11)** (1999), 3181–3187.

Received June 2005; revised January 2006.

E-mail address: britta.nestler@hs-karlsruhe.de
E-mail address: denis.danilov@hs-karlsruhe.de